**Indonesian Journal of Electrical Engineering and Informatics (IJEEI)**
Vol. 12, No. 1, March 2024, pp. 179~194
ISSN: 2089-3272, DOI: 10.52549/ijeei.v12i1.5372 

# Fuzzy Logic Based DTC Control of Synchronous Reluctance Motor

**Sayed O. Madbouly**
Department of Electrical Engineering, College of Engineering, Qassim University, Saudi Arabia.

**Article Info**

***Article history:***

Received Jan 8, 2024
Revised Feb 18, 2024
Accepted Mar 20, 2024

***Keyword:***

*Synchronous Reluctance Motor,*
*Fuzzy Logic Control, Direct Torque Control,*
*Speed Control,*
*Electrical Machines.*

**ABSTRACT**

This paper presents the utilization of a fuzzy logic controller (FLC) within the speed control loop of the direct torque control (DTC) algorithm. The aim is to enhance the dynamic performance of a 3-phase synchronous reluctance motor (SynRM) in variable speed applications. The proposed FLC employs the speed error and change of speed error to generate the torque command signal needed for the torque hysteresis comparator within the DTC scheme. The system being analyzed comprises of a synchronous reluctance motor, voltage source converter and the proposed fuzzy logic-based DTC. In order to evaluate the performance of the proposed controller, a comprehensive system model is developed and simulated using MATLAB Simulink. The dynamic response of the entire system is investigated when subjected to various command speeds and loading conditions. It is found that the proposed controller achieves fast and precise dynamic response under all operating conditions. Furthermore, a comparative analysis is conducted between utilizing the FLC and the traditional proportional integral differential (PID) controller in the speed control loop of the DTC, the results demonstrate a significant improvement in the dynamic response when employing FLC compared to the traditional PID controller.



***Corresponding Author:***

Sayed O. Madbouly,
Department of Electrical Engineering,
College of Engineering,
Qassim University, Saudi Arabia
Email: **so.ossman@qu.edu.sa**, **sayed_madpouly@hotmail.com**

## 1. INTRODUCTION

Recently, the Synchronous Reluctance Motor has emerged as a promising substitute for conventional 3-PH induction motors and permanent magnet synchronous motors in variable speed applications that prioritize high efficiency, cost-effectiveness, and reliability. This motor exhibits numerous advantages, including the absence of rotor windings and permanent magnets, a sturdy rotor construction, no excitation necessity, negligible speed regulation, superior power density, and heightened efficiency [1-5]. Furthermore, its pricing is comparable to that of induction motor drives, making it a competitive option in terms of cost [6,7].

Several high-performance control techniques have been developed and implemented in SynRM motors, including field-oriented control (FOC) and DTC. The strategy of FOC is based on decoupling the stator current in a coordinate system that rotates synchronously with the magnetic flux into two components, the d-axis component, responsible for controlling the flux, and the q-axis component, responsible for controlling the torque [8-10]. FOC requires coordinate transformation to transform the stator three phase currents from stationary reference frame to synchronously rotating reference frame in which d-axis is coincides with rotor flux space vector. Additionally, it requires pulse width modulation (PWM) to generate the stator voltage signals, that drive the motor [11,12]. The field-oriented control approach has good dynamic torque and flux characteristics, but it is complicated since it has modulator blocks and coordinate transformation in its structure.

Compared to alternative vector control techniques, the DTC technique has a number of benefits. It discards the requirement for coordinate transformations, a current controller, and a pulse width modulator.

Additionally, it offers precise and quick dynamic response and lessens reliance on machine parameters [13,14]. With DTC, the decupled control of torque and flux is obtained by proper selection of stator space voltage vector [15,16].

The conventional DTC employs PID controller in the speed control loop [17], the disadvantages of PID controller are the complexity of tuning especially for complex systems, sensitivity to Model Changes, struggle to adapt to changing operating conditions and parameters variations, integral action can experience integrator windup during significant changes in set point [18].

A very powerful expert system method with applications in many control domains is fuzzy logic control. It overcomes the drawbacks of conventional PI controllers and provides increased system robustness. Fuzzy logic control, in contrast to traditional control techniques, does not require a thorough mathematical model of the system. Rather, it builds a rule-based system by utilizing the knowledge of the overall behavior and operation of the system. Fuzzy logic control can improve system performance and adapt to complex and uncertain contexts without the need for exact mathematical models [19-25].

In this research paper a proposed FLC is employed in the speed control loop, the outer control loop, of the DTC algorithm to enhance the dynamic behavior of SynRM in the variable speed application. The performance the proposed controller is investigated under various command speeds and load conditions, encompassing both transient and steady-state operation.

## 2. MODELLING OF SYNCHRONOUS RELUCTANCE MOTOR

In this paper, the model of SynRM is developed under the following assumptions:

1. Considering a linear magnetic circuit and disregarding saturation effects.
2. Assuming sinusoidal distribution for the stator winding.
3. No Damper Bars in the Rotor

The space vector equations of SynRM in stationary reference frame are given as follows

$$\underline{v}_{s\alpha\beta} = \underline{i}_{s\alpha\beta} R_s + \frac{d\underline{\psi}_{s\alpha\beta}}{dt} \quad (1)$$

$$\underline{\psi}_{s\alpha\beta} = \underline{i}_{s\alpha\beta} L_s \quad (2)$$

$$T = \underline{i}_{s\alpha\beta} \; x \; \underline{\psi}_{s\alpha\beta} \quad (3)$$

By the aid of the SynRM circuit representation illustrated in Fig. 1, the space vector model of the motor referred to rotor reference frame, which rotates by an electrical angular velocity of e, can be derived as follows

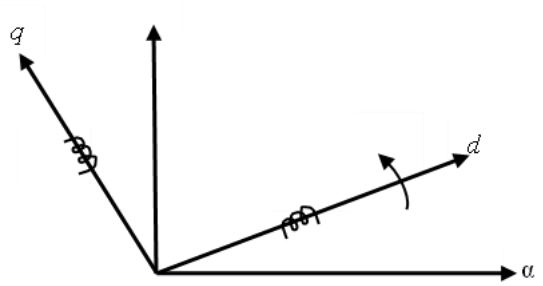


Figure 1. Circuit representation of SynRM

$$\underline{v}_{sdq} = \underline{i}_{sdq} R_s + \frac{d\underline{\psi}_{sdq}}{dt} + j\omega_e \underline{\psi}_{sdq} \quad (4)$$

$$\underline{\psi}_{sdq} = \underline{i}_{sdq} L_s \quad (5)$$

$$T = \underline{i}_{sdq} \; x \; \underline{\psi}_{sdq} \quad (6)$$

Expanding the previous space vector equations, into d-q axis, the SynRM model in the rotor reference can be expressed as follows [26,27]:

$$v_{sd} = i_{sd} R_s + \frac{d\psi_{sd}}{dt} - \omega_e \psi_{sq} \quad (7)$$

$$v_{sq} = i_{sq} R_s + \frac{d\psi_{sq}}{dt} + \omega_e \psi_{sd} \quad (8)$$

$$\psi_{sd} = i_{sd} L_{sd} \quad (9)$$
$$\psi_{sq} = i_{sq} L_{sq} \quad (10)$$

Where:

$v_{sd}$ and $v_{sq}$: d-q components of stator space voltage vector.

$\psi_{sd}$ and $\psi_{sq}$: d-q components of stator flux vector.

$L_{sd}$ and $L_{sq}$ : d-q values of stator inductance.

$i_{sd}$ and $i_{sq}$ : d-axis and q-axis components of the stator space current vector.

$R_s$ :value of the stator windings' resistance.

$\omega_e$ : electrical angular velocity.

The motor developed torque and motor dynamic equation of motion can be expressed as follows

$$T_e = \frac{3}{2}\frac{p}{2}(L_{sd} - L_{sq}) i_{sd} i_{sq} \quad (11)$$
$$T_e - \beta\omega_r - T_L = J\frac{d\omega_r}{dt} \quad (12)$$

Where:

$p$ is the number of poles, $\omega_r$ is the angular mechanical speed, $T_L$ is the mechanical load torque, $\beta$ is the friction coefficient, and J is the moment of inertia.

## 3. DTC CONCEPTS

The primary objective of DTC is to attain independent and simultaneous control of the stator magnetic flux and developed torque in the motor. This is accomplished by selecting the most appropriate stator voltage vector from the available voltage vectors of voltage source converter and applying it to the stator three phase windings. In SynRM, the torque equation can be expressed in terms of the stator magnetic flux and current space vectors as follows:

$$T = \frac{3}{2}\frac{p}{2}\,\underline{\psi_s} \times \underline{i_s} = \frac{3}{8} p \frac{(L_{sd} - L_{sq})}{L_{sd} L_{sq}} |\psi_s|^2 \, sin\, sin\, (2\delta) \quad (13)$$

Where:

$\underline{i_s}$ and $\underline{\psi_s}$ represent the stator space current and flux vector respectively, while $\delta$ represents the flux angle.

Based on Equation 13, it can be inferred that the modulation of the motor's developed torque is achievable by keeping the stator flux linkage constant while rapidly adjusting the stator flux angle (δ). This adjustment is made possible by choosing a suitable stator voltage vector from the voltage source inverter.
In a stationary reference frame, the relationship between the stator flux and stator voltage can be represented by the following equation.

$$\underline{\psi_s} = \int \left(\underline{v_s}(t) - R_s \underline{i_s}\right) dt \quad (14)$$

When neglecting the voltage drop due to stator resistance and assuming a small sampling period (Δt), Equation 14 can be expressed in the following form

$$\underline{\psi_s}(t + \Delta t) = \underline{\psi_s}(t) + \underline{v_s}\, \Delta t \quad (15)$$

Equation 15 is represented graphically in Fig. 2., which shows that the tangential component of the voltage vector ($\underline{v_s}\, \Delta t$) influences the flux angle which subsequently governs the torque. On the other hand, the radial component controls the flux's magnitude.

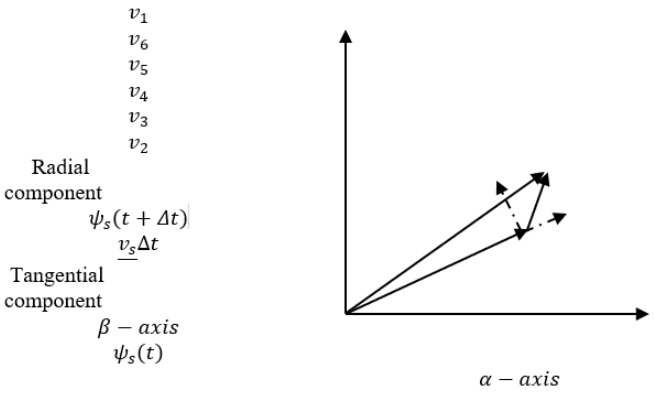


Figure 2. Inverter voltage vectors and space flux vector

As shown in Fig.3, the DTC algorithm comprises of three primary blocks. The first block represents the stator flux and torque hysteresis comparators, which compares the estimated values of torque and flux ($T_e$ and $\psi_s$) with their reference values ($T^*$ and $\psi_s^*$). The output of the hysteresis controllers reflects the desired state of both torque and flux (ST and Sψ). The torque status is represented by three discrete values: 1 signifies increasing torque, -1 denotes decreasing torque, and 0 indicates no action. Similarly, the flux status has two possible configurations, 1 and -1.

The second block in the DTC algorithm is referred to as the optimal switching logic. It utilizes the torque and flux status information, along with the spatial location (θ) of the stator flux vector, to identify the inverter switching states (Sa, Sb, Sc). These switching states are corresponding to the optimal stator voltage vector which achieves both flux and torque status. Table 1, outlines how the optimal voltage vector is selected based on the flux/torque status and the sector in which the flux is positioned in space. Fig. 4, depicts the spatial division of the space into six sectors.

The third block of DTC is the adaptive motor model, which calculates the actual torque, stator flux magnitude, and its spatial position. These calculations are based on the states of the inverter switches, inverter DC link voltage ($v_{dc}$), and two-phase stator current.

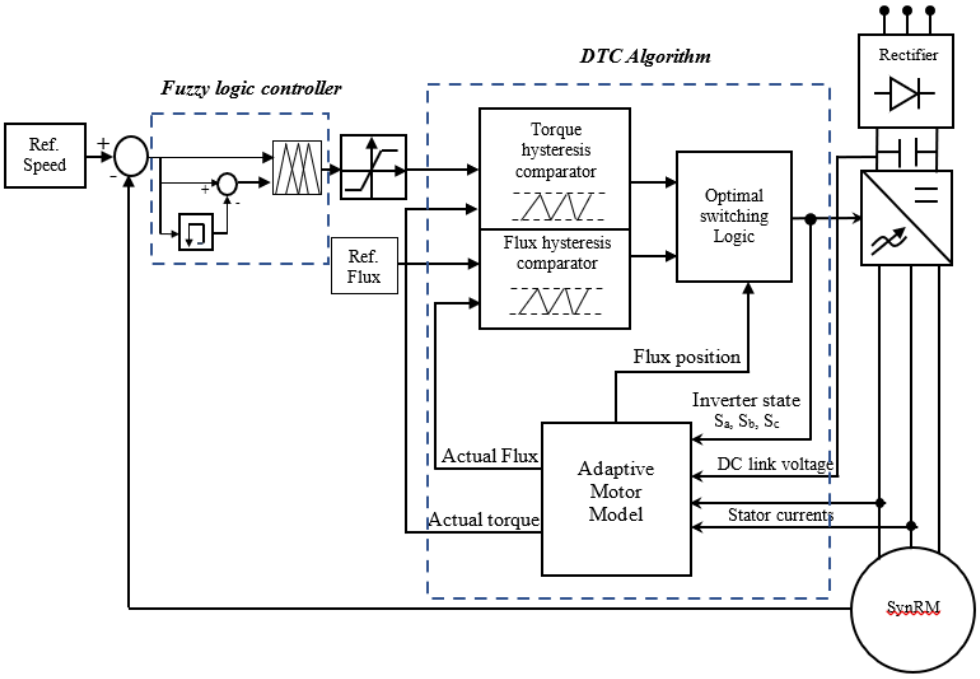


Figure 3. Schematic diagram of the proposed controller

Table 1. Optimum switching rules

| $S_T$ , $S_\psi$, θ(n) | | $\theta_1$ | $\theta_2$ | $\theta_3$ | $\theta_4$ | $\theta_5$ | $\theta_6$ |
|---|---|---|---|---|---|---|---|
| $S_\psi$= 1 | $S_T$ =1 | $v_2$ | $v_3$ | $v_4$ | $v_5$ | $v_6$ | $v_1$ |
| | $S_T$ =0 | $v_7$ | $v_8$ | $v_7$ | $v_8$ | $v_7$ | $v_8$ |
| | $S_T$ = -1 | $v_6$ | $v_1$ | $v_2$ | $v_3$ | $v_4$ | $v_5$ |
| $S_\psi$= 0 | $S_T$ =1 | $v_3$ | $v_4$ | $v_5$ | $v_6$ | $v_1$ | $v_2$ |
| | $S_T$ =0 | $v_8$ | $v_7$ | $v_8$ | $v_7$ | $v_8$ | $v_7$ |
| | $S_T$ = -1 | $v_5$ | $v_6$ | $v_1$ | $v_2$ | $v_3$ | $v_4$ |

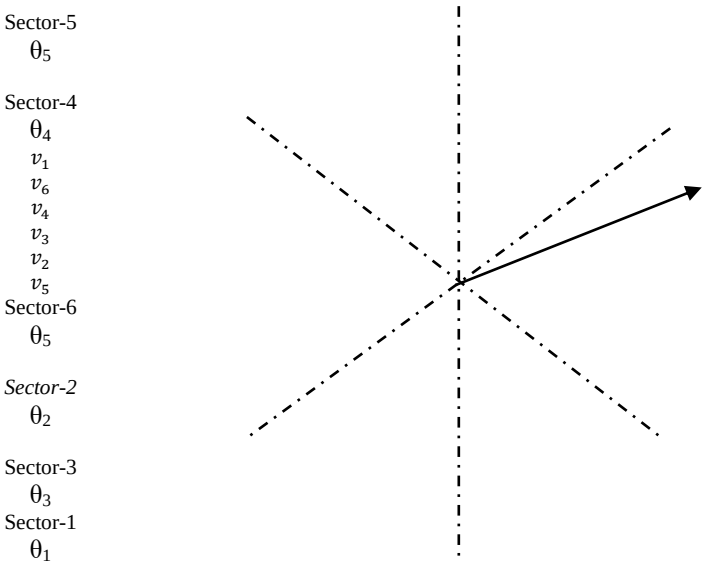


Figure. 4. Spatial division of the space

Equations 16 and 17 are employed in the adaptive motor model to estimate the stator voltage vector and stator current vector in the stationary reference frame. After obtaining the stator voltage and current vectors, the adaptive motor model employs equations 18 and 19 to estimate the magnitude of the stator magnetic flux ($|\psi_s|$), the position of the stator flux (Θ), and the magnitude of the torque (T).

$$\underline{v_s} = \frac{2}{3}\, v_{dc}(s_a + s_b a + s_c a^2) = v_{s\alpha} + v_{s\beta} j \tag{16}$$

$$\underline{i_s} = \frac{2}{3}\, (i_a + i_b a + i_c a^2) = i_{s\alpha} + i_{s\beta} j \tag{17}$$

$$\underline{\psi_s} = \int \left(\underline{v_s}(t) - R_s \underline{i_s}\right) dt = \psi_{s\alpha} + \psi_{s\beta} j = |\psi_s| e^{j\theta} \tag{18}$$

$$T = \frac{3}{2} p(\psi_{s\alpha} i_{s\beta} - \psi_{s\beta} i_{s\alpha}) \tag{19}$$

Where $a = e^{\frac{2\pi}{3}}$

## 4. Fuzzy Inference System

The fuzzy inference system (FIS) which is employed in this study is based on Mamdani's system as shown in Fig.5, this FIS consists of three main parts

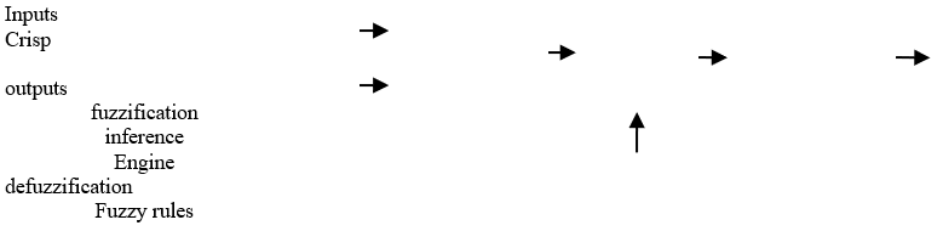


Figure 5. fuzzy system structure

### 4.1. Fuzzification of input variables.

The fuzzification is the process of converting crisp, precise inputs variables into fuzzy inputs that can be effectively processed by the fuzzy logic system. To achieve fuzzification, the universe of discourse for the input variable (U) is divided into multiple fuzzy sets, each possessing a linguistic label and a corresponding membership function. Each crisp input $x$ is converted to a fuzzy input by determining its degree of membership ($\mu$), value between 0 and 1, of all associated fuzzy sets. As shown in Fig. 6, for a crisp input of (-3) the results of fuzzification is 0.9-degree membership of (Low) fuzzy set, 0.5-degree membership of (Medium) fuzzy set and 0-degree of membership of (high) fuzzy set.

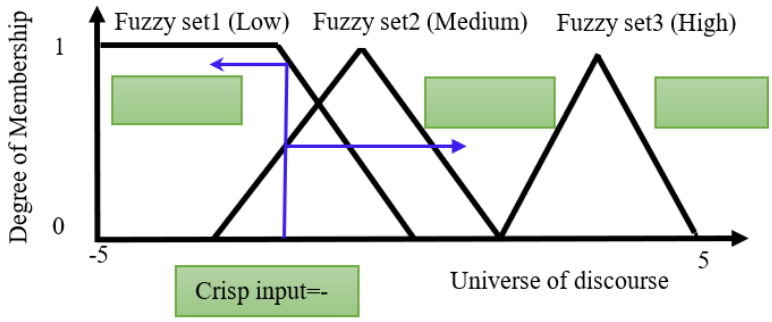


Figure 6. Fuzzification process

There are various types of membership functions that can be used for fuzzification, such as triangular, trapezoidal, Gaussian, sigmoidal, and singleton. The choice of membership function depends on the nature of the input variable and the specific requirements of the fuzzy logic system. For example, triangular membership functions are commonly used for inputs with clear boundaries, while Gaussian functions are useful for capturing smooth transitions.

### 4.2. Fuzzy rules and fuzzy operators.

Fuzzy rules form the basis of control strategy of the system and are usually derived from expert knowledge or heuristics. These rules are based on "if-then" concept. Once the input data has been fuzzified and their corresponding membership values have been determined, these membership values are used as antecedents to the fuzzy rules. In case of a fuzzy rule has multiple antecedents, a fuzzy operator, such as the minimum(AND) or maximum (OR) is applied to obtain a single numerical value, the resulting value truncates the output fuzzy set of the rule. For each fuzzy output, all the outputs of the fuzzy rules are aggregated into a single fuzzy set known as aggregated output fuzzy set, as depicted in Fig. 7.

### 4.3. Defuzzification of fuzzy outputs

The last step in a fuzzy logic system is defuzzification, in this process the aggregated output fuzzy set is converted to a crisp output. Various methods, known as defuzzifiers, can be utilized for this purpose, including the centroid, bisector, mean of maximum, largest of maximum, and smallest of maximum.

One widely used defuzzifier is the centroid method. In this approach, the crisp output is determined as the center of the area located beneath the aggregated fuzzy set. This can be visualized in Fig. 7, where the crisp output is positioned at the centroid of the fuzzy set.

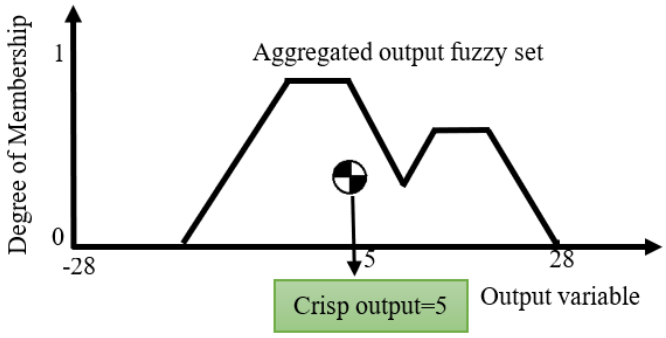


Figure 7. Defuzzification Process

### 4.4. Proposed fuzzy logic controller

The proposed FLC is employed as a speed controller in the speed control loop of the DTC algorithm, as depicted in Fig. 3. The input state variables to the controller are chosen to be the normalized speed error (Δω) and the rate of change of speed error ($\Delta\omega$·). Seven fuzzy sets are employed to cover the universe of discourse of speed error input, five of them have triangular membership functions and the remaining two have trapezoidal membership functions as shown in Fig.8. They are denoted by the linguistic terms positive high (ph), positive medium (pm), positive small (ps), zero (z), negative small (ns), negative medium (nm) and negative high (nh). While, three fuzzy sets are employed for the rate of change of speed error, one has a triangular membership function and the remaining are of trapezoidal membership function as illustrated in Fig.9, the linguistic representation of them are, negative (n), zero (z), and positive (p). The proposed FLC has one output state variable, represent the incremental change in the command torque( $\Delta T^*$), a seven fuzzy sets have been utilized through the output range from -28 N.m. to 28 N.m., there linguistic terms are positive high (ph), positive medium (pm), positive small (ps), zero (z), negative small (ns), negative medium (nm) and negative high (nh) as illustrated in Fig.10.

The proposed FIS consists of 21 fuzzy rules detailed in Table 2. Each rule is associated with two input membership functions. The output of the fuzzy rules is evaluated using the minimum operator (AND). The centroid defuzzifier, shown in Fig.11, is used for the defuzzification process. Additionally, Fig. 12 displays a plot of the fuzzy rule surface.

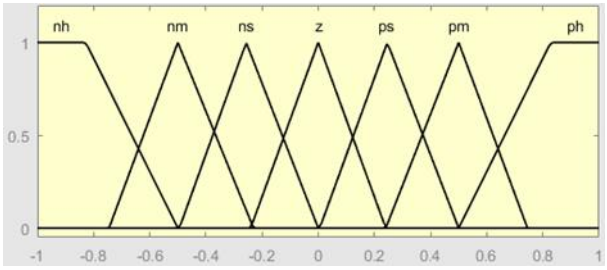


Figure 8. MFs of Speed Error Input (Δω)

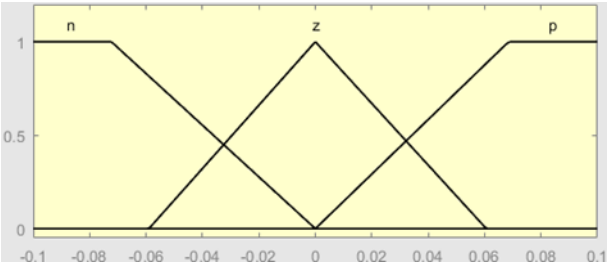


Figure 9. MFs of the Chang of Speed Error ($\Delta\dot{\omega}$)

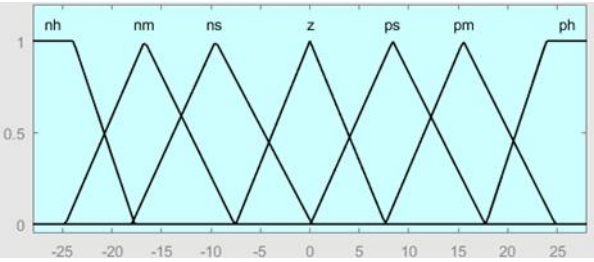


Figure 10. MFs of the incremental torque ($\Delta T^*$)

Table 2. Fuzzy control system rules for proposed Mamdani's system

| *Change of speed error* | *Speed error* | | | | | | |
|---|---|---|---|---|---|---|---|
| | **nh** | **nm** | **ns** | **z** | **ps** | **pm** | **ph** |
| **n** | nh | nh | nh | z | pm | pm | ph |
| **z** | nh | nh | ns | z | pm | ph | ph |
| **p** | nh | nm | ns | ps | ph | ph | ph |

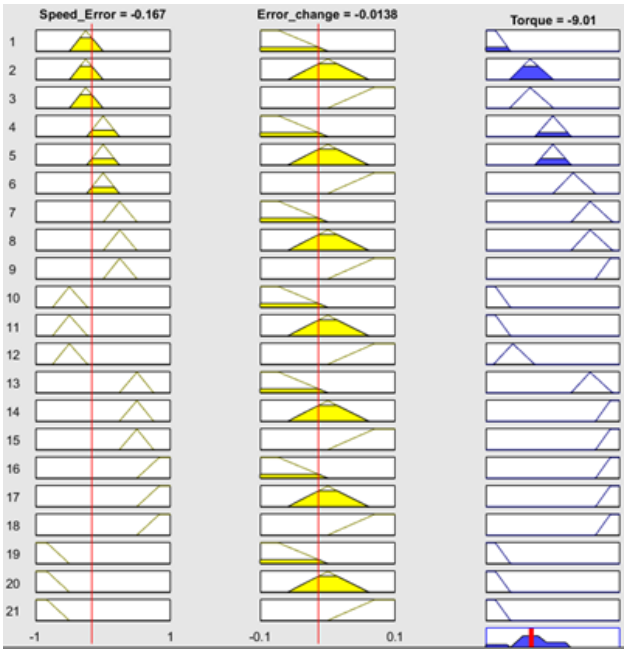


Figure 11. View of rules, fuzzification and defuzzification of proposed Mamdani's FIS

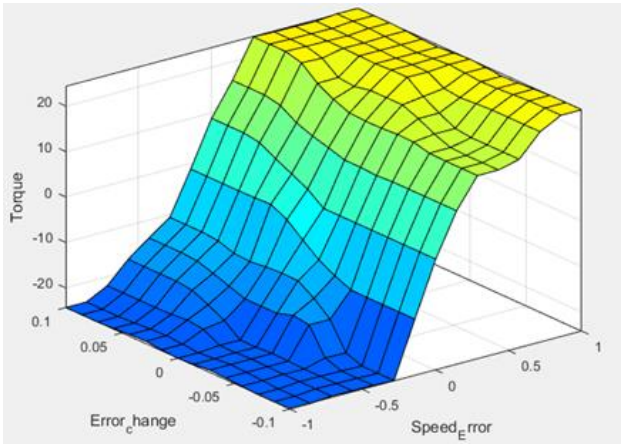


Figure 12. Rule surface view of proposed Mamdani's FIS

## 5. SIMULATION RESULTS

In order to assess the dynamic performance of SynRM under the proposed controller, a comprehensive system model is developed and simulated using MATLAB Simulink. The simulations are carried out under various command speed and different loading conditions.

In the simulations, a sampling period of 50 μs is employed, along with a constant reference flux (ψ*) of 0.9 Wb. The DC link voltage of the inverter ($E_{dc}$) is maintained at 560 V throughout the simulations. Table 3, presents the numerical values corresponding to the motor parameters.

Table 3. Parameters of SynRM

| | |
|---|---|
| Rated Power | 2.2KW |
| $L_{sd}$ | 0.159H |
| $L_{sq}$ | 0.039H |
| $R_s$ | 1.72Ω |
| $p$ | 4 |
| J | 0.0017 Kg.m$^2$ |
| B | 0.14 N.m /rad/s |

### 5.1. Simulation results for successive step change of reference speed under full load

$$V_{cd} = R_{sc}\, i_{cd} + \left(L_{sc} - \frac{L_{hc}^2}{\sigma L_r}\right)\frac{di_{cd}}{dt} + \frac{R_r L_{sp} L_{hc}}{\sigma L_{hc} L_r} i_{pd} - \left[\omega_{sl}\left(L_c - \frac{L_{hc}^2}{\sigma L_r}\right) - p_2\,\omega_r L_{sc}\right] i_{cq} - p_2\,\omega_r \frac{L_{hc} L_{sp}}{L_{hp}} i_{pq} - \frac{R_r L_{hc}}{\sigma L_{hp} L_r}\left|\Psi_p\right|$$

The dynamic performance of the proposed system is investigated through simulation involving sequential step change in command speed under full load conditions. The motor is initially started at 500 rpm step command speed. At t=0.4 s, a step-up change occurs, increasing the command speed from 500 rpm to 1000 rpm. Finally, at t=0.8 s, another step-up change takes place, raising the command speed from 1000 rpm to 1500 rpm

Fig. 13. Depicts the motor speed response, it is evident that the actual speed exhibits a rise from zero to 500 rpm within a rise time of 75 ms. The settling time is observed to be 110 ms. The peak time, representing the time taken to reach the first peak speed, is found to be 110.7 ms. Notably, there is minimal overshoot, with only a 1 rpm increase, accounting for a mere 0.2% deviation from the command speed.

when the command speed is altered from 500 rpm to 1000 rpm at t=0.4 s, the motor speed exhibits a rapid response, closely tracking the command speed. The rise time is determined to be 80 ms, settling time is 100 ms, peak time is 101 ms. Notably, there is minimal overshoot, with only a slight increase of 0.7 rpm, accounting for a mere 0.07% deviation from the command speed.

Finally, when the command speed changes from 1000 rpm to the full load speed of 1500 rpm, the rise time is found to be 0.09s, settling time is 0.109 s and the peak time is 0.1095 s. The overshoot is small, with only a slight increase of 0.69 rpm, accounting for a mere 0.045% deviation from the command speed.

Fig. 14. Shows the load torque and motor developed torque, it can be illustrated that the torque exhibits fluctuations or ripples during steady-state operation. These torque ripples have a peak-to-peak value of 5.5 N.m.

Fig. 15, illustrates the behavior of the stator 3-phase currents. It can be observed that the current magnitude reaches 5A rms at full load, Moreover, as the motor speed rises, the frequency of the current waveform also increases.

Fig. 16, illustrates the magnitude of the rotating field. It can be noticed that the flux closely follows the command value. However, there are flux ripples present with a peak-to-peak value of 0.05 Wb which represent approximately 5.5% of the steady-state value.

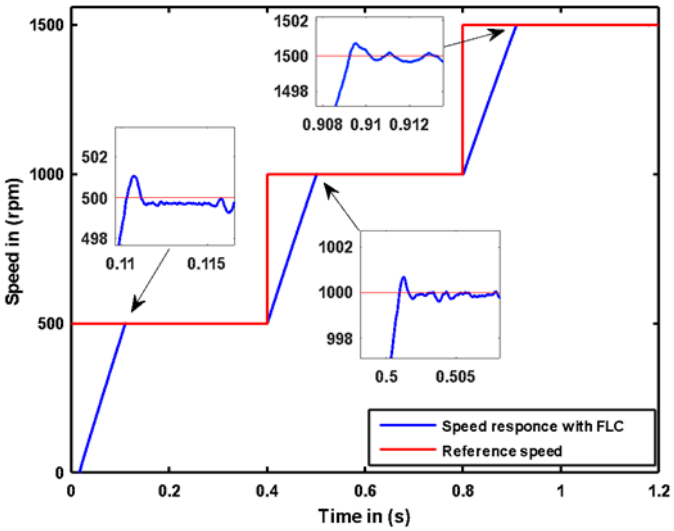


Figure 13. Command speed and motor speed response

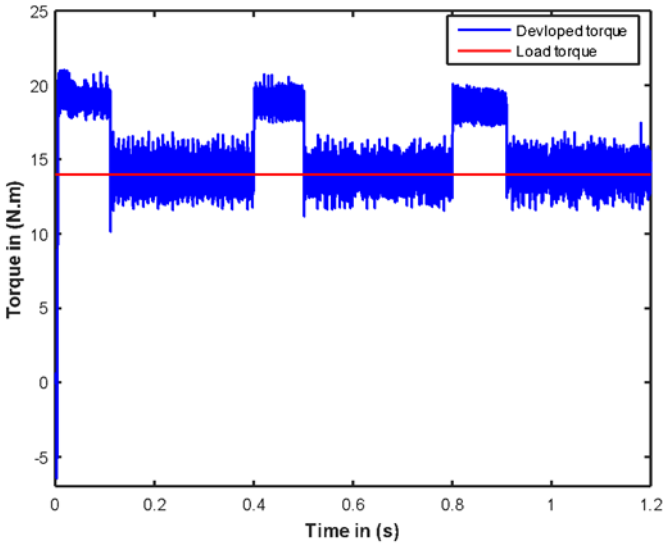


Figure 14. Developed torque response and load torque

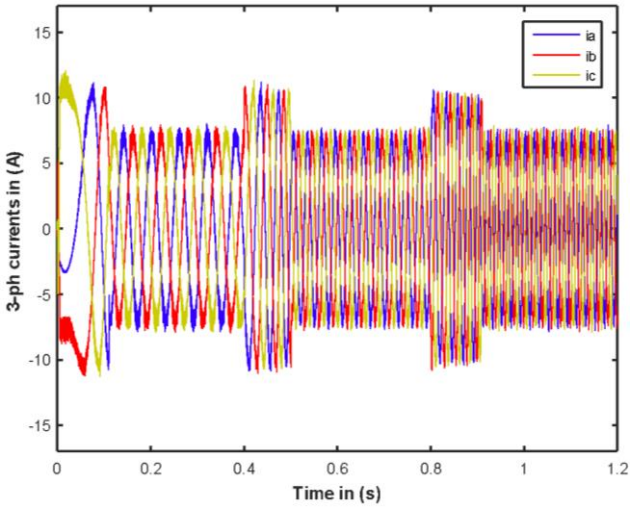


Figure 15. 3-phase currents

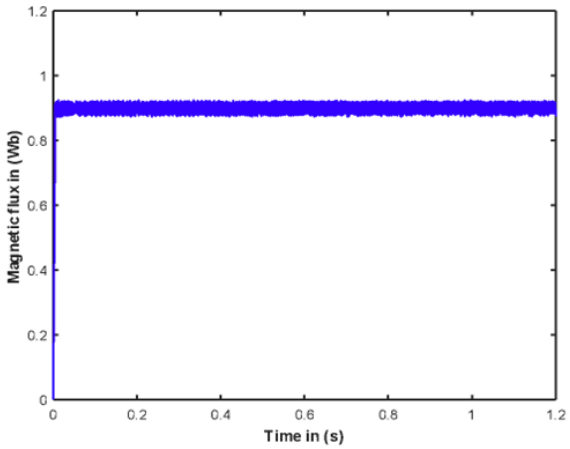


Figure 16. Stator flux magnitude currents

**5.2. Simulation results for step command speed and sudden load variations.**

In this case, the system being analyzed initiates with a step-up reference speed of 1500 rpm under no load conditions. At t=0.4 s, a sudden application of full load torque occurs, followed by its removal at t=0.8 s.

Fig. 17. depicts the motor speed response and the corresponding command speed, revealing that the motor speed accurately follows the reference speed. Furthermore, the steady-state error is nearly negligible under both full load and no-load conditions.

Upon the sudden application of full load torque at t=0.4 s, a minor undershoot of 39 rpm is observed, which corresponds to a mere 2.6% deviation from the steady-state speed. Similarly, when the torque is suddenly removed, the speed response demonstrates a minimal overshoot of 4 rpm, representing only 0.26% of the steady-state speed.

Fig.18. illustrates the load torque and motor developed torque while Fig.19. illustrates the per phase stator current.

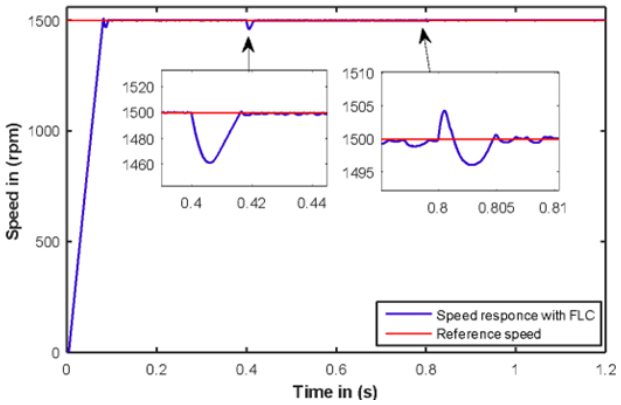


Figure 17. Command speed and motor speed response

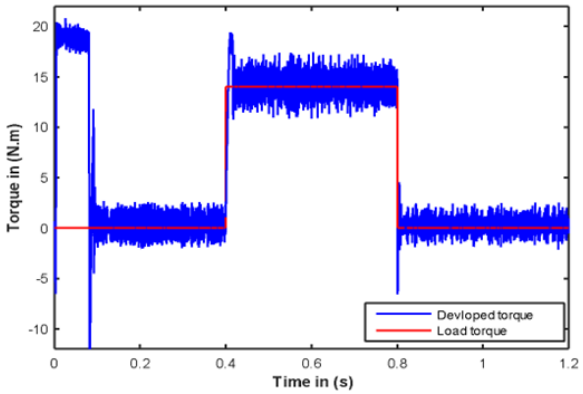


Figure 18. Load torque and motor developed torque

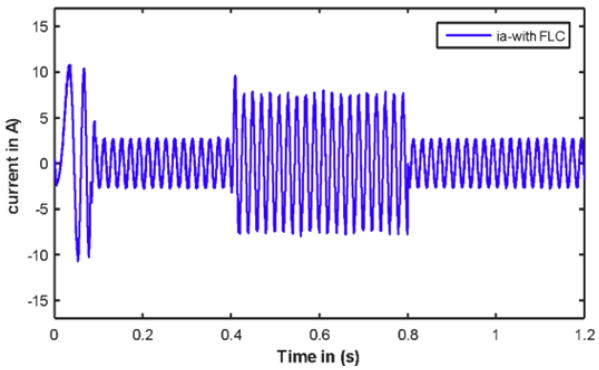


Figure 19. stator per phase current

### 5.3. Comparative Analysis of Dynamic Responses between Fuzzy Logic and Traditional PID Controllers

In this case, a traditional PID controller is implemented in the speed control loop of the DTC algorithm rather than the fuzzy logic controller. A comparative analysis is conducted to evaluate the dynamic response of the proposed system when operated with either the PID controller or the fuzzy logic controller.

Fig. 20 illustrates the speed response of the system under full load torque when subjected to successive command speed changes. A comparison between the system response with the FLC and the conventional PID controller reveals that the fuzzy logic controller exhibits improved performance in terms of settling time and steady-state error.

Furthermore, Fig. 21 illustrates the system's response to a step command speed of 1500 rpm under no load conditions, followed by sudden load application and subsequent removal. Comparing the system responses with the FLC and the PID controller, it is observed that the fuzzy logic controller outperforms the PID controller in terms of setting time, steady-state error, and the percentage of overshoot/undershoot.

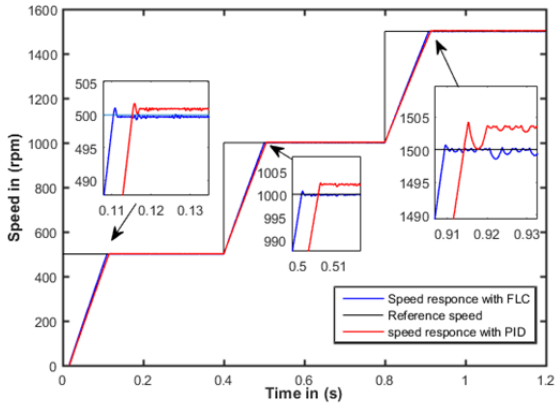


Figure 20. Speed response with FLC and PID controller under sequential step change of command speed.

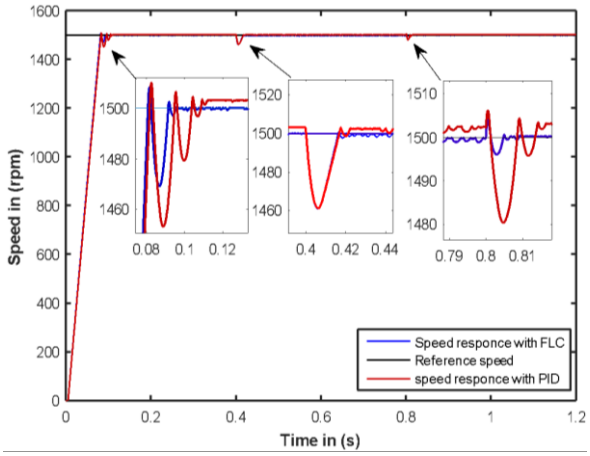


Figure 21. Speed response with FLC and PID controller with load variations

### 5.4. Comparison between system response of Sugeno and Mamdani FIS

In this section, a Sugeno fuzzy inference system is developed for system control. The proposed Sugeno system includes two inputs and one output. The inputs are the speed error and rate of change of speed error, which are represented by seven and three fuzzy sets, respectively. The output is the incremental change of torque, which is described by five membership functions corresponding to linguistic terms: nh (negative high), nm (negative medium), ns (negative small), ps (positive small), pm (positive medium), and ph (positive high). A total of 21 rules are formulated and appropriately designed in the FIS, as presented in Table 4. The rules viewer is depicted in Fig. 22, while the rules surface is illustrated in Fig. 23.

The system response for a sequential speed command, shown in Figure 24, indicates that the performance of the system using the proposed Mamdani system outperforms the proposed Sugeno system in terms of steady-state error. However, both systems exhibit similar characteristics in terms of rise time and settling time.

Table 4. Fuzzy control system rules for proposed Sugeno FIS

| *Change of speed error* | *Speed error* | | | | | | |
|---|---|---|---|---|---|---|---|
| | **nh** | **nm** | **ns** | **z** | **ps** | **pm** | **ph** |
| **n** | nh | nh | nh | z | Ps | ps | ps |
| **z** | nh | ns | ns | z | ps | ps | ph |
| | ns | ns | ns | z | ph | ph | ph |
| **p** | | | | | | | |

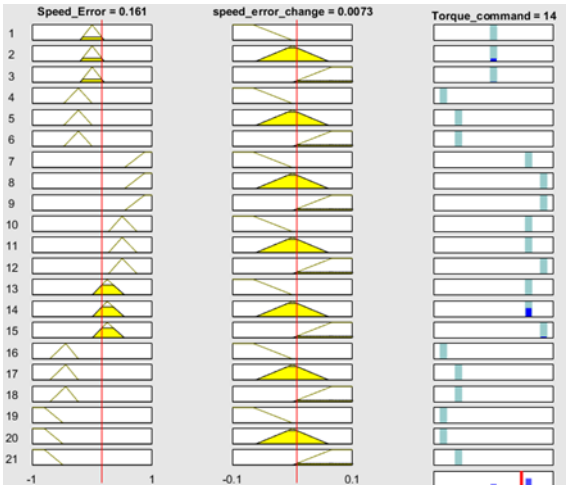


Figure 22. View of rules, fuzzification and defuzzification of proposed Mamdani FIS

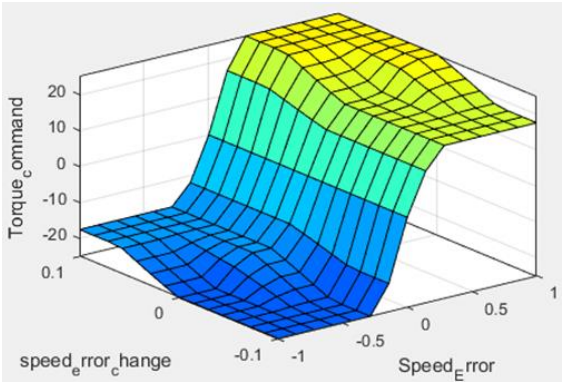


Figure 23. Rule surface view of proposed Sugeno FIS

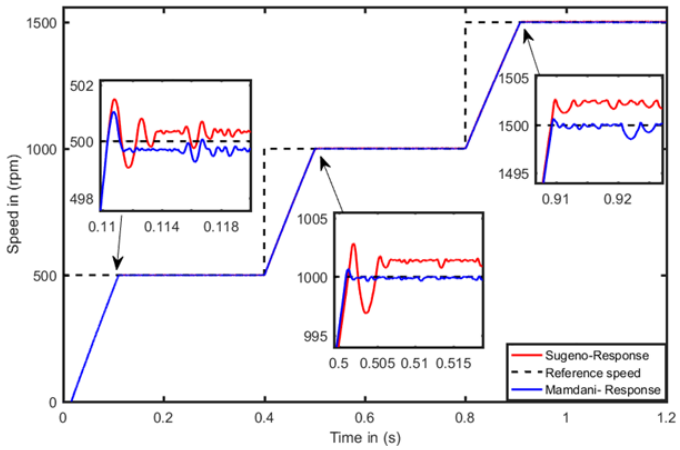


Figure 24. Speed response for the proposed Mamdani's and Sugeno FIS

### 5.5. Effect of changing the membership functions

The dynamic response of the system was investigated when the membership functions of the input/output fuzzy variables are changed from triangular to Gaussian, as depicted in Fig.25. Fig. 26 displays the speed response of the system to sequential changes in speed commands. It can be observed that the dynamic speed response of the system with triangular membership functions exhibits a slight improvement compared to that with Gaussian membership functions in terms of rise time and steady state error.

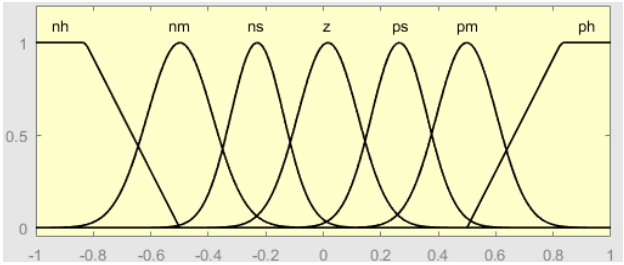


(a)

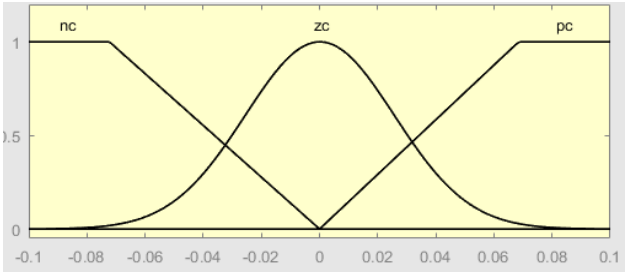


(b)

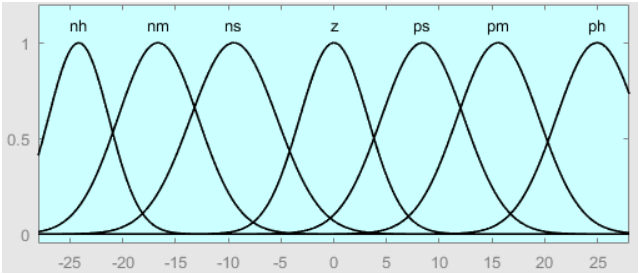


(c)

Figure 25 a: MFs for speed error input b: MFs for rate of speed error c: output MFs

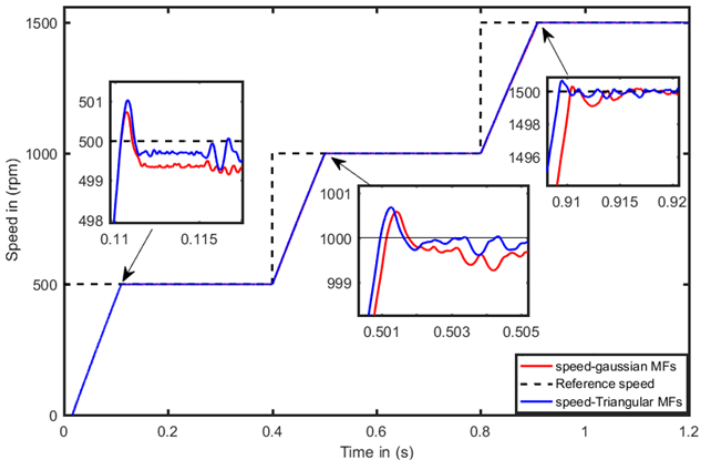


Figure 26. speed response for Triangular and Gaussian MFs

### 5.6. Comparison of the proposed controller and its findings in this study and other related research studies.

In this section, a comparative study between the proposed controller in this research and other related studies is presented. The fuzzy logic controller proposed in this paper utilizes seven fuzzy membership functions for the speed error and incorporates 21 fuzzy rules. In contrast, [25] employs five membership functions and 15 fuzzy rules in their approach. Furthermore, while the FLC in this paper is utilized as a speed controller, [26] replaces hysteresis comparators and optimal switching logic with FLC in their study. Additionally, in [27], the DTC controller incorporates a conventional PI controller, resulting in a slower dynamic response compared to the approach introduced in this paper.

## 6. CONCLUSION

The implementation of the fuzzy logic-based DTC control system for the speed control of SynRM is presented in this paper. In the DTC algorithm's speed control loop, outer control loop, the traditional PID controller is replaced with a fuzzy logic controller.

To evaluate the effectiveness of the proposed controller, a simulation analysis is carried out using MATLAB/Simulink software. The dynamic response of the proposed system is tested when subjecting the SynRM to various reference speed and load conditions. The results demonstrate that the fuzzy logic controller produces fast and accurate dynamic response, characterized by minimal overshoot, small steady state error and small rise time. Also, it is found that the FLC outperforms the traditional PID controller providing a better dynamic response for the SynRM speed control application. The future work which can be added is conducting comparative studies with other control strategies, such as model predictive control (MPC) or artificial neural network (ANN), can provide a comprehensive understanding of the strengths and weaknesses of the fuzzy logic controller in comparison to alternative control approaches.

## REFERENCES

[1] De Almeida, A.T.; Ferreira, F.J.T.E.; Baoming, G. Beyond induction motors—Technology trends to move up efficiency. IEEE Trans. Ind. Appl. 2014, 50, 2103–2114.

[2] Boztas, G., Aydogmus, O. & Guldemir, H. Design and implementation of a high-efficiency low-voltage synchronous reluctance motor. Electr Eng 104, 717–725 (2022).

[3] Y. Okamoto, R. Hoshino, S. Wakao and T. Tsuburaya, "Improvement of Torque Characteristics for a Synchronous Reluctance Motor Using MMA-based Topology Optimization Method," in IEEE Transactions on Magnetics, vol. 54, no. 3, pp. 1-4, March 2018, Art no. 7203104, doi: 10.1109/TMAG.2017.2762000.

[4] M. -Y. Wei and T. -H. Liu, "Design and Implementation of an Online Tuning Adaptive Controller for Synchronous Reluctance Motor Drives," in IEEE Transactions on Industrial Electronics, vol. 60, no. 9, pp. 3644-3657, Sept. 2013, doi: 10.1109/TIE.2012.2206341.

[5] Asad, B.; Vaimann, T.; Belahcen, A.; Kallaste, A.; Rassõlkin, A.; Iqbal, M.N. Broken rotor bar fault detection of the grid and inverter-fed induction motor by effective attenuation of the fundamental component. IET Electr. Power Appl. 2019, 13, 2005–2014.

[6] Wu, G.; Huang, S.; Wu, Q.; Rong, F.; Zhang, C.; Liao, W. Robust predictive torque control of N*3-phase PMSM for high-power traction application. IEEE Trans. Power Electron. 2020, 35, 10799–10809.

[7] Du, G.; Zhang, G.; Li, H.; Hu, C. Comprehensive Comparative Study on Permanent-Magnet-Assisted Synchronous Reluctance Motors and Other Types of Motor. Appl. Sci. 2023, 13, 8557. https://doi.org/10.3390/app13148557

[8] Costin, M.; Lazar, C. Field-Oriented Predictive Control Structure for Synchronous Reluctance Motors. Machines 2023, 11, 682. https://doi.org/10.3390/machines11070682

[9] H. A. A. Awan, M. Hinkkanen, R. Bojoi and G. Pellegrino, Stator-Flux-Oriented Control of Synchronous Motors: A Systematic Design Procedure, IEEE Transactions on Industry Applications, vol. 55, no. 5, Sept.-Oct. 2019, pp. 4811-4820, doi: 10.1109/TIA.2019.2927316.
[10] A. Varatharajan, G. Pellegrino and E. Armando, Direct Flux Vector Control of Synchronous Motor Drives: A Small-Signal Model for Optimal Reference Generation, IEEE Transactions on Power Electronics, vol. 36, no. 9, pp. 10526-10535, Sept. 2021, DOI: 10.1109/TPEL.2021.3067694.
[11] Wang, F.; Zhang, Z.; Mei, X.; Rodríguez, J.; Kennel, R. Advanced Control Strategies of Induction Machine: Field Oriented Control, Direct Torque Control and Model Predictive Control. Energies 2018, 11, 120. https://doi.org/10.3390/en11010120
[12] Costin, M.; Lazar, C. Field-Oriented Predictive Control Structure for Synchronous Reluctance Motors. Machines 2023, 11, 682. https://doi.org/10.3390/machines11070682
[13] Wang, F.; Zhang, Z.; Mei, X.; Rodríguez, J.; Kennel, R. Advanced Control Strategies of Induction Machine: Field Oriented Control, Direct Torque Control and Model Predictive Control. Energies 2018, 11, 120. https://doi.org/10.3390/en11010120
[14] M. Abdelouhab, A. Attar, A. Senhaji, R. Aboutni, J. Bouchnaif, Improved direct torque control on an induction machine with short circuit fault, Materials Today: Proceedings, Volume 72, Part 7, 2023.
[15] sayed o. madbouly "Torque/Speed Control of 3PH Synchronous Reluctance Motor Using Direct Torque Control" International Review of Electrical Engineering (IREE), Vol. 17 no. 4, August 2022.
[16] I. Pavlić, Š. Ileš, I. Erceg and M. Kutija, "Predictive Direct Torque Control of SynRM in Field Weakening Region," 2021 IEEE 19th International Power Electronics and Motion Control Conference (PEMC), Gliwice, Poland, 2021, pp. 574-580, doi: 10.1109/PEMC48073.2021.9432594.
[17] Gudey, S.K.; Malla, M.; Jasthi, K.; Gampa, S.R. Direct Torque Control of an Induction Motor Using Fractional-Order Sliding Mode Control Technique for Quick Response and Reduced Torque Ripple. World Electr. Veh. J. 2023, 14, 137. https://doi.org/10.3390/wevj14060137
[18] T. Sreekumar and K. S. Jiji, "Comparison of Proportional-Integral (P-I) and Integral-Proportional (I-P) controllers for speed control in vector controlled induction Motor drive," 2012 2nd International Conference on Power, Control and Embedded Systems, Allahabad, India, 2012, pp. 1-6, doi: 10.1109/ICPCES.2012.6508089.
[19] Kakouche, K.; Oubelaid, A.; Mezani, S.; Rekioua, D.; Rekioua, T. Different Control Techniques of Permanent Magnet Synchronous Motor with Fuzzy Logic for Electric Vehicles: Analysis, Modelling, and Comparison. Energies 2023, 16, 3116. https://doi.org/10.3390/en16073116
[20] S. O. Madbouly, H. F. Soliman, H. M. Hasanien and M. A. Badr, "Fuzzy logic control of brushless doubly fed induction generator," 5th IET International Conference on Power Electronics, Machines and Drives (PEMD 2010), Brighton, UK, 2010, pp. 1-7, doi: 10.1049/cp.2010.0085.
[21] V. T. Ha, "Torque Control of an In-Wheel Axial Flux Permanent Magnet Synchronous Motor using a Fuzzy Logic Controller for Electric Vehicles", Eng. Technol. Appl. Sci. Res., vol. 13, no. 2, pp. 10357–10362, Apr. 2023.
[22] S. O. Madbouly, H. F. Soliman, H. M. Hasanien and M. A. Badr, "Fuzzy logic control of brushless doubly fed induction generator," 5th IET International Conference on Power Electronics, Machines and Drives (PEMD 2010), Brighton, UK, 2010, pp. 1-7, doi: 10.1049/cp.2010.0085.
[23] Kolluru, Ashok & Kumar, M.. (2022). Fuzzy Controller Based DTC of SRM Drive Fed by Common High Side Asymmetric Switch Converter. International journal of electrical and computer engineering systems. 13. 701-708. 10.32985/ijeces.13.8.10.
[24] Kakouche, Khoudir, Adel Oubelaid, Smail Mezani, Djamila Rekioua, and Toufik Rekioua. 2023. "Different Control Techniques of Permanent Magnet Synchronous Motor with Fuzzy Logic for Electric Vehicles: Analysis, Modelling, and Comparison" *Energies* 16, no. 7: 3116. https://doi.org/10.3390/en16073116
[25] V.K., Arun Shankar & Subramaniam, Umashankar & Paramasivam, Sathesh & Padmanaban, Sanjeevikumar & Kommanaboina, Venkatesh. (2018). Investigation of Direct Torque Control-Based Synchronous Reluctance Motor Drive for Pumping. 10.1007/978-981-10-4762-6_30.
[26] W. Zhao, D. Chen, and T. A. Lipo, Performance improvement of ferrite-assisted synchronous reluctance machines using asymmetrical rotor configurations, IEEE Transactions on Magnetics, vol. 51, no. 11, Nov. 2015, Art. ID. 8108504.
[27] H. A. A. Awan, M. Hinkkanen, R. Bojoi and G. Pellegrino, Stator-Flux-Oriented Control of Synchronous Motors: A Systematic Design Procedure, IEEE Transactions on Industry Applications, vol. 55, no. 5, Sept.-Oct. 2019, pp. 4811-4820, doi: 10.1109/TIA.2019.2927316.

## BIOGRAPHIES OF AUTHORS

Sayed O. Madbouly received the B.Sc., M.Sc., and Ph.D. degrees in Electrical Engineering from Ain Shams University, Egypt, in 1998, 2004, and 2010 respectively. From 2010 to 2013, he is an Assistant Professor in the Electrical Power and Machines Department, Faculty of Engineering, Ain Shams University, Egypt. Since 2013, he is an Assistant Professor in the Electrical Engineering Department, College of Engineering, Qassim University, Saudi Arabia. His major research interests include electrical machines, renewable energy, and control of electrical machines.
E-mails: so.ossman@qu.edu.sa & sayed_madpouly@hotmail.com